An Islanding Detection Method for Inverter-Based Distributed Generators Based on the Reactive Power Disturbance

Xiaolong Chen and Yongli Li

***Abstract*—In this paper, an islanding detection method for inverter-based distributed generators (DGs) is presented, which is based on perturbing reactive power output. Two sets of disturbances are configured in this method, which have different amplitudes and duration time. The first set of reactive power disturbance (FSORPD) is periodic with small amplitudes to break the reactive power balance during islanding, whereas the magnitude of the second set of reactive power disturbance (SSORPD) is sufficient to force the frequency to deviate outside its threshold limits. Considering all the possible frequency variation characteristics with the FSORPD after islanding, three criterions are designed for switching the disturbance from the FSORPD to the SSORPD. Since DGs located at different positions have the same frequency variation characteristics, the SSORPDs can be added on different DGs at the same time without the need of communication. Therefore, synchronization of the SSORPDs can be guaranteed for the system with multiple DGs and the method can detect islanding with a zero nondetection zone property. Moreover, the method can be applied to the DG either operating at unity power factor or supplying reactive power as well for its local load. According to the antiislanding test system recommended in IEEE Std.929-2000 and IEEE Std.1547-2003, the effectiveness of the method has been validated with several case studies in the power systems computer-aided design/Electro magnetic transient in DC system environment.**

***Index Terms*—Disturbance synchronization, inverter-based distributed generation, islanding detection, reactive power disturbance.**

I. Introduction

THE inverter-based distributed generator (DG) uses renewable energy (photovoltaic, wind power, fuel cell, and microturbine, etc.) to supply power for the network and local load [1], [2]. It is being widely applied to protect environment and make the power industry development sustainable. In order to ensure the safe operation of both the network and the DG, the DG has to be equipped with islanding detection function according to IEEE Std. 929-2000 and IEEE Std. 1547-2003 [3], [4].

Manuscript received February 6, 2015; revised April 27, 2015 and June 17, 2015; accepted July 20, 2015. Date of publication July 29, 2015; date of current version December 10, 2015. This work was supported in part by the Project supported by the National Basic Research Program of China (973 Program) under Award 2009CB219704, and in part by the Program of National Natural Science Foundation of China under Award 51177108. Recommended for publication by Associate Editor Prof. H. Li.

The authors are with the Key Laboratory of Smart Grid of Ministry of Education, Tianjin University, Tianjin 300072, China (e-mail: promising1207@163.com; lyltju@163.com).

Color versions of one or more of the figures in this paper are available online at http://ieeexplore.ieee.org.

Digital Object Identifier 10.1109/TPEL.2015.2462333

Islanding is a condition in which a portion of the utility system that contains both the DG and load continues operating while this portion is electrically separated from the main utility. Unintentional islanding can result in power quality problems, serious equipment damage, and even safety hazards to utility operation personnel [5], [6]. Therefore, the DG has to detect islanding effectively in this case and disconnect itself from the network as soon as possible to prevent the damages mentioned earlier. According to IEEE Std. 929-2000 and IEEE Std. 1547-2003, a maximum delay of 2 s is required for the detection of an islanding and a generic system for islanding detection study is recommended as well, where the distributed network, the *RLC* load and the DG are connected at the point of common coupling (PCC).

Generally, islanding detection methods can be classified into following three categories: 1) communication-based methods; 2) passive methods; and 3) active methods. Communication-based methods do no harm to the power quality of the power system and have no nondetection zones (NDZs) in the theory. However, the cost is much high because of the need of communication infrastructure and the operations are more complex as well [7]. In addition, the effectiveness cannot be guaranteed with the risk of communication breakdown [8]. Therefore, passive and active methods have been well developed.

Passive methods determine the islanding condition by measuring system parameters such as the magnitude of the voltage at the PCC, the PCC voltage frequency, and phase jump [9]. Accordingly, over/under frequency protection (OFP/UFP), over/under voltage protection (OVP/UVP) and phase jump detection (PJD) are the most widely used passive islanding detection methods. These passive methods are easy to implement and do no harm to the power quality, but they may fail to detect islanding when the local load's power consumption closely matches the DG's power output [10], [11].

In order to reduce or eliminate the NDZ, active methods rely on intentionally injecting disturbances, negative sequence components or harmonics into some DG parameters to identify whether islanding has occurred [12]–[14]. The active frequency drift [15], slip-mode frequency shift [16], and Sandia frequency shift [17] methods are three classical active methods by creating a continuous trend to change the frequency during islanding. Though active methods suffer smaller NDZs, they sacrifice power quality and reliability of the power system during normal operation. Moreover, some active methods have difficulty in maintaining synchronization of the intentional disturbances. Therefore, they may not work owing to

the averaging effect when applied in multiple-DG operation [18], [19].

Recently, schemes based on reactive power control to detect islanding are attractive and several methods have been proposed [20]–[27]. In order to detect islanding, the basic mechanism of these methods is to create the reactive power mismatch, which can drive the frequency of the PCC voltage to change during islanding. This can be achieved only by redesigning reactive power reference for the DG or injecting reactive power/current disturbance, which can be easily implemented. Moreover, the NDZ can be reduced or even eliminated with proper design.

The idea in this paper is inspired by the studies in [22] and [23]. An islanding detection method based on intermittent bilateral reactive power variation (RPV) was proposed in [22]. The variation amplitude was 5% of the DG's active power output. The frequency was eventually forced to deviate outside the normal range during islanding due to the reactive power variation. Compared with the method in [22], the method proposed in [23] was improved by only outputting unilateral RPV in each variation period and further reducing the variation amplitude based on the load's resonance frequency detection. However, both methods suffered a serious problem, which was that the synchronization of the RPVs could not be guaranteed when the methods were applied to multiple DGs. Therefore, the effectiveness of the methods was reduced and they might fail to detect islanding for the system with multiple DGs. On the other hand, the DG was also explored to generate both active and reactive power simultaneously for power factor improvement [28], [29], as well as the voltage regulation [25], [30]. The islanding detection methods proposed in [20] and [25] were designed for the DG of this kind. However, the methods proposed in [22] and [23] were appropriate only for the DG operating at unity power factor.

For the DG generating both active and reactive power, the relationship between the reactive power disturbance and the frequency variation during islanding is analyzed in this paper, which is different from that for the DG operating at unity power factor. Moreover, this paper presents an innovative islanding detection method, which is based on perturbing reactive power output as well. Two sets of disturbances are configured, which have different amplitudes and duration time. The first set of reactive power disturbance (FSORPD) is periodic with small amplitudes, whereas the magnitude of the second set of reactive power disturbance (SSORPD) is sufficient to force the frequency to deviate outside its threshold limits during islanding. Considering all the possible frequency variation characteristics with the FSORPD after islanding, three criterions are designed for switching the disturbance from the FSORPD to the SSORPD. Since DGs located at different positions have the same frequency variation characteristics, the SSORPDs on different DGs can be activated at the same time without the need of communication. Therefore, the proposed method has following three distinguishing features: 1) It can be applied to the DG either operating at unity power factor or supplying reactive power as well for its local load; 2) The perturbation of reactive power is further reduced during normal operation; 3) Synchronization of the disturbances can be guaranteed for the system with multiple DGs and the method can detect islanding with the zero NDZ property.

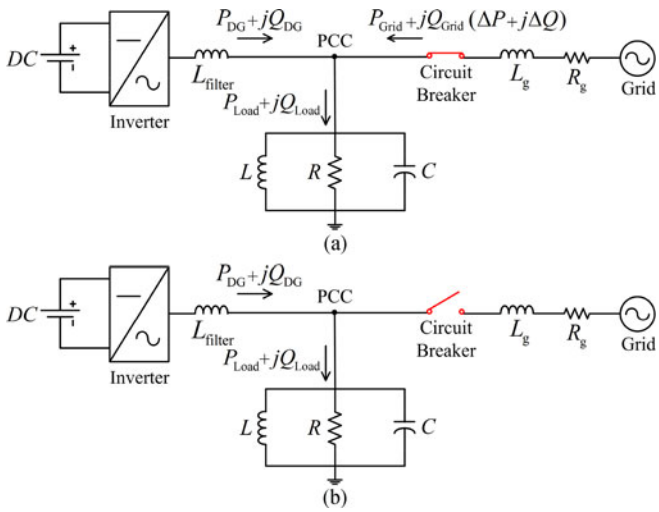

Fig. 1. Test system for islanding detection study (a) Grid-connected operation mode (b) Islanding operation mode.

II. Basic Relationship Analysis and RPV Methods

A. System Modeling and Basic Relationship Analysis

According to IEEE Std.929 and IEEE Std.1547, the recommended test system for islanding detection study is shown in Fig. 1. It consists of an inverter-based DG, a parallel *RLC* load and the grid represented by a source behind impedance. The operation mode of the DG depends on whether the circuit breaker is closed or not.

The Inverter-based DG such as photovoltaic generation and wind power generation is usually configured with the maximum power point tracking controller. Since the islanding detection time is very short, the output power can be considered to be constant during the detection. Therefore, using a constant dc source behind a three-phase inverter, the DG is designed as a constant power source.

Fig. 2 presents the block diagram of the DG interface control. The phase-locked loop (PLL), the outer power control loop and the inner current control loop are three main parts. According to the instantaneous power theory and the Park transformation, the DG can control the active and reactive power output independently based on the dual close loop control structure in the *d-q* synchronous reference frame [25].

As shown in Fig. 1(a), when the DG is connected to the utility grid, the following equations describe the power flows and the active and reactive power consumed by the load:

$$P_{\mathrm{Load}} = P_{\mathrm{DG}} + P_{\mathrm{Grid}} = 3\frac{V_{\mathrm{PCC}}^2}{R} \tag{1}$$

$$Q_{\mathrm{Load}} = Q_{\mathrm{DG}} + Q_{\mathrm{Grid}} = 3V_{\mathrm{PCC}}^2\left(\frac{1}{2\pi fL} - 2\pi fC\right) \tag{2}$$

where V_{PCC} and f are the phase voltage at the PCC and its frequency, and R, L, C represent the load resistance, inductance, and capacitance, respectively. Moreover, the load's resonant

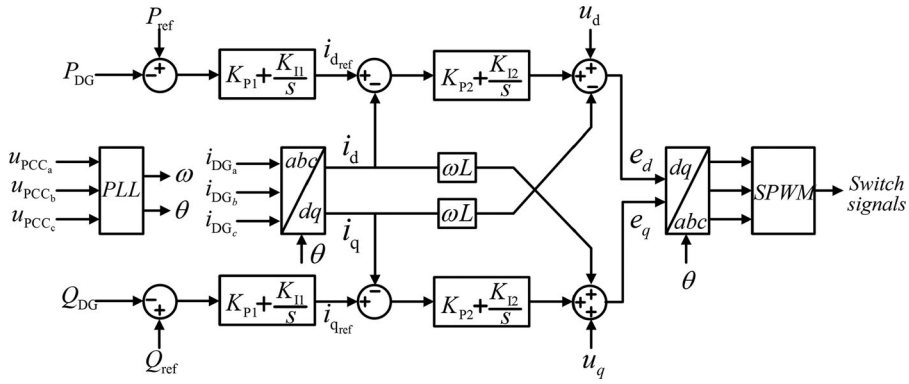

Fig. 2. DG interface control for constant power operation.

frequency (f_0) and quality factor (Q_f) can be expressed as

$$f_0 = \frac{1}{2\pi\sqrt{LC}} \tag{3}$$

$$Q_f = R\sqrt{\frac{C}{L}} = 2\pi f_0 RC. \tag{4}$$

According to IEEE Std.929, Q_f is typically set at 2.5. By combining (1), (3), and (4), (2) can be rewritten as follows:

$$Q_{\mathrm{Load}} = P_{\mathrm{Load}} Q_f \left(\frac{f_0}{f} - \frac{f}{f_0}\right). \tag{5}$$

On the other hand, when islanding occurs as shown in Fig. 1(b), it can be inferred from (1) that if the active power mismatch $\Delta P(\Delta P = P_{\mathrm{Load}} - P_{\mathrm{DG}} = P_{\mathrm{Grid}})$ is not equal to zero, the PCC voltage will fall or rise no matter the DG operates at unity power factor or not. The amount of voltage deviation depends on the value of ΔP. If the active power reference of the DG is set to be constant, ΔP can be expressed as follows [11]:

$$\Delta P = P_{\mathrm{DG}} \left(\frac{1}{(1+\Delta V)^2} - 1\right) \tag{6}$$

where ΔV represents the voltage deviation and it can be expressed as

$$\Delta V = \frac{V_{\mathrm{PCC}.i} - V_{\mathrm{PCC}}}{V_{\mathrm{PCC}}} \tag{7}$$

where V_{PCC} and $V_{\mathrm{PCC}.i}$ represent the PCC voltage before and after islanding, respectively. According to IEEE Std.929 and IEEE Std.1547, the voltage thresholds are typically set at 88% and 110% of the rated voltage value. If the active power mismatch is not large enough, the passive OVP/UVP method will suffer the NDZ due to inadequate changes of the PCC voltage [11]. Assuming that there is no active power mismatch during islanding, it can be inferred from (6) that the values of the disturbance on the DG's active power reference to drive the voltage to exceed its upper and lower thresholds are at least $-17.4\%P_{\mathrm{DG}}$ and $29.1\%P_{\mathrm{DG}}$, respectively.

Similarly, it can be seen from (5) that the reactive power mismatch $\Delta Q\,(\Delta Q = Q_{\mathrm{Load}} - Q_{\mathrm{DG}} = Q_{\mathrm{Grrid}})$ causes the frequency variation once islanding occurs. Thus, the frequency variation also can be used to detect islanding based on the OFP/UFP method. Power consumed by the load is equal to that generated by the DG during islanding. According to (5), the load's reactive power consumption after islanding ($Q_{\mathrm{Load}.i}$) can be expressed as follows:

$$\begin{aligned} Q_{\mathrm{Load}.i} &= Q_{\mathrm{DG}} = P_{\mathrm{Load}.i} Q_f \left(\frac{f_0}{f_i} - \frac{f_i}{f_0}\right) \\ &= P_{\mathrm{DG}} Q_f \left(\frac{f_0}{f_i} - \frac{f_i}{f_0}\right) \end{aligned} \tag{8}$$

where $P_{\mathrm{Load}.i}$ and f_i represent the load's active power consumption and the frequency of the PCC voltage after islanding, respectively.

The DG operating at unity power factor does not generate reactive power. As for the DG of this kind, it can be inferred from (8) that the value of f_i is equal to that of f_0. If f_i is within the frequency's threshold limits, which are typically set at 49.3 and 50.5 Hz (50 Hz is the rated frequency) according to IEEE Std.929 and IEEE Std.1547, the passive OFP/UFP method will suffer the NDZ. In order to eliminate the NDZ in this condition, perturbation on the DG's reactive power reference is necessary as well to force the frequency to exceed its threshold limits. According to (8), the needed reactive power disturbance to force the frequency to deviate from f_i to its target value (Q_{dis}) can be expressed as follows:

$$Q_{\mathrm{dis}} = P_{\mathrm{DG}} Q_f \left(\frac{f_0}{f_i + \Delta f} - \frac{f_i + \Delta f}{f_0}\right) \tag{9}$$

where Δf represents the frequency deviation and it can be expressed as

$$\Delta f = f_{i.\mathrm{tar}} - f_i \tag{10}$$

where $f_{i.\mathrm{tar}}$ represents the target frequency and it can be set at any value that is out of the frequency's normal range. For the DG operating at unity power factor, assuming that P_{DG} is equal to 1, Fig. 3 illustrates the relationship between f_i and Q_{dis} with $f_{i.\mathrm{tar}}$ being set at the threshold values. It can be seen from Fig. 3 that: 1) the Q_{dis}–f_i curve shows the approximately linear characteristic for the period between 49.3 Hz and 50.5 Hz and 2) the values of Q_{dis} to force the frequency to exceed its upper and lower thresholds are at least $-5\%P_{\mathrm{DG}}$ and $7\%P_{\mathrm{DG}}$

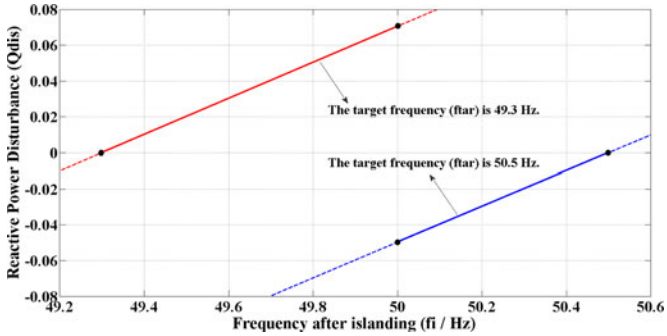

Fig. 3. Relationship between f_i and $Q_{\rm dis}$ for the DG operating at unity power factor.

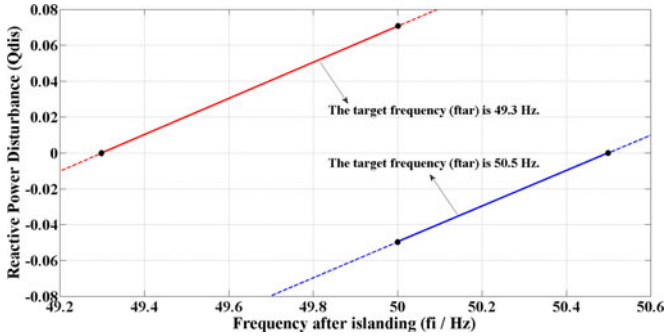

Fig. 4. Relationship between f_i and $Q_{\rm dis}$ for the DG generating both active and reactive power (f_0 is set at 50 Hz).

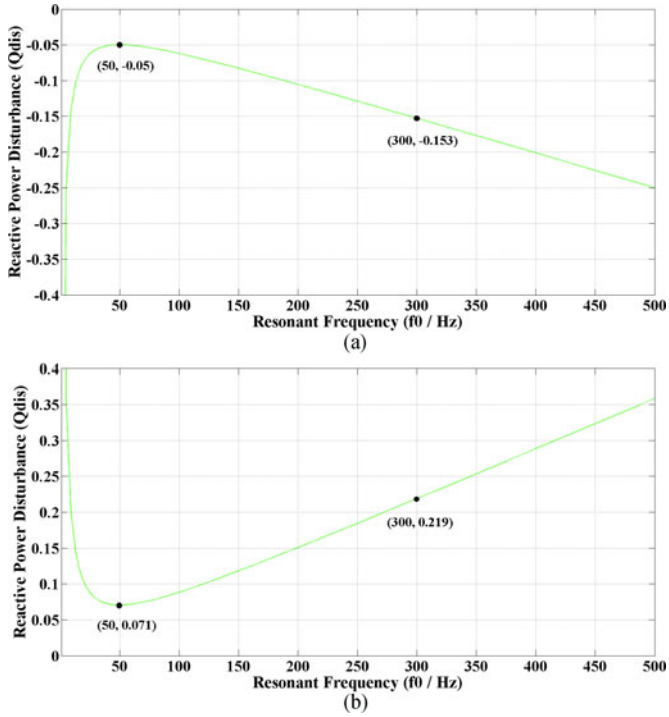

Fig. 5. Relationship between f_0 and $Q_{\rm dis}$ for the DG generating both active and reactive power (a) f_i and $f_{i\rm tar}$ are set at 50 Hz and 50.5 Hz, respectively (b) f_i and $f_{i\rm tar}$ are set at 50 Hz and 49.3 Hz, respectively.

respectively, which are much less than those of the active power disturbance to drive the voltage to exceed its limits.

However, the relationship between $Q_{\rm dis}$ and Δf should be modified when the DG supplies both active and reactive power for the local load. If there are no power mismatches, the frequency will not change after islanding. According to (8), $Q_{\rm dis}$ for the DG of this kind can be expressed as follows:

$$\begin{aligned} Q_{\rm dis} &= P_{\rm DG}Q_f\left(\frac{f_0}{f_{i.\rm tar}}-\frac{f_{i.\rm tar}}{f_0}\right)-P_{\rm DG}Q_f\left(\frac{f_0}{f_i}-\frac{f_i}{f_0}\right) \\ &= -P_{\rm DG}Q_f\Delta f\left(\frac{f_0}{f_i(f_i+\Delta f)}+\frac{1}{f_0}\right). \end{aligned} \tag{11}$$

Compared with the value of f_i for the DG operating at unity power factor, it is not necessarily equal to that of f_0 here. Moreover, though parameters of $P_{\rm DG}$, Q_f, and $f_{i.\rm tar}$ can be definitely obtained or set, it can be seen from (11) that the relationship between f_i and $Q_{\rm dis}$ is still uncertain. That is because the value of f_0 is unknown in advance. Therefore, two conditions are considered to analyze the relationship among f_0, f_i, and $Q_{\rm dis}$. *Condition 1:* Assuming that $P_{\rm DG}$ is equal to 1 and f_0 is equal to 50 Hz, Fig. 4 illustrates the relationship between f_i and $Q_{\rm dis}$ with $f_{i.\rm tar}$ being set at the threshold values. Compared with Fig. 3, Fig. 4 shows approximately the same $Q_{\rm dis}$–f_i curve. *Condition 2:* Assuming that $P_{\rm DG}$ is equal to 1 and f_i is equal to 50 Hz, Fig. 5 illustrates the relationship between f_0 and $Q_{\rm dis}$ with $f_{i.\rm tar}$ being set at the threshold values. It can be seen from Fig. 5 that: 1) when f_0 is equal to 50 Hz, the absolute values of $Q_{\rm dis}$ to force f_i to deviate to its threshold limits are approximately the smallest and 2) the $Q_{\rm dis}$–f_0 curve shows the approximately linear characteristic for the range where f_0 is larger than 50 Hz. Therefore, following two important conclusions can be obtained: 1) for the load whose resonant frequency f_0 is actually unknown in advance, the calculated $Q_{\rm dis}$ might be not sufficient enough to drive f_i to deviate to $f_{i.\rm tar}$ with f_0 being set at 50 Hz in (11) and 2) for the same load, the frequency variation with f_0 being set at 300 Hz is about three times as much as that with f_0 being set at 50 Hz.

B. Islanding Detection Methods Proposed in [22] and [23] Based on the RPV

Owing to the smaller disturbance amplitude analyzed previously, islanding detection methods based on the reactive power disturbance might be better choices than those based on the active power disturbance. The authors in [22] and [23] presented islanding detection methods for the DG operating at unity power factor based on intermittently bilateral and unilateral reactive power variations, respectively. Moreover, the upper and lower thresholds of the frequency were set at 50.5 Hz and 49.5 Hz according to China GB/T 19939-2005.

In [22], the DG's reactive power reference ($Q_{\rm ref}$) switched among three different values in each variation period, which could be expressed as follows:

$$Q_{\rm ref}=\begin{cases} Q_{\rm dis}, & 0\le t<T_{+Q} \\ -Q_{\rm dis}, & T_{+Q}\le t<T_{+Q}+T_{-Q} \\ 0, & T_{+Q}+T_{-Q}\le t<T_{\rm dis} \end{cases} \tag{12}$$

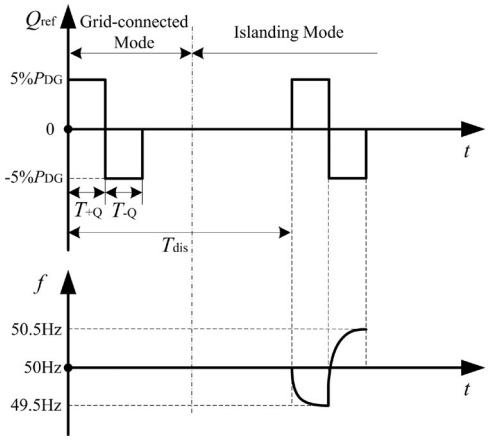

Fig. 6. $Q_{\rm ref}$ and corresponding frequency in both operation modes with the method proposed in [22].

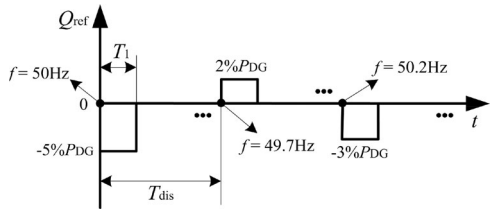

Fig. 7. Reactive power reference of the DG with different values of the frequency in [23].

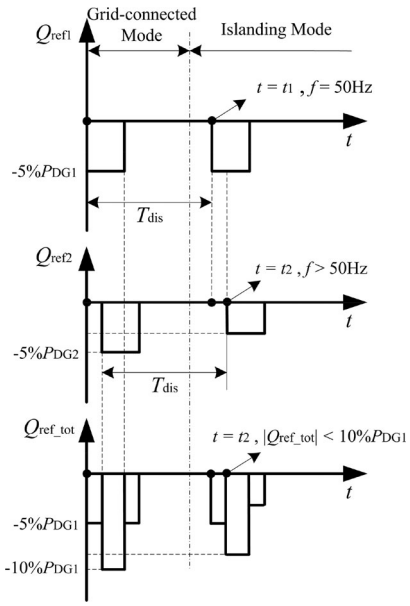

Fig. 8. Separate and total reactive power variations for the system with two DGs according to the method in [23].

where T_{+Q} and T_{-Q} were the duration time for $Q_{\rm dis}$ and $-Q_{\rm dis}$, respectively, and $T_{\rm dis}$ is the variation period. Moreover, $Q_{\rm dis}$ was equal to $5\%P_{\rm DG}$, which was basically adequate to force the frequency to deviate outside its limits. For the load whose f_0 is equal to 50 Hz, Fig. 6 illustrated $Q_{\rm ref}$ and corresponding frequency in both grid-connected and islanding modes, respectively.

Compared with the method in [22], the improved RPV method in [23] only output unilateral reactive power variation in each variation period. Moreover, the variation could adaptively change its amplitude based on the load's resonance frequency detection. When the frequency at the beginning of the variation was not equal to 50 Hz, the variation amplitude was less than $5\%P_{\rm DG}$, thus reducing the variation as much as possible. According to the method in [23], $Q_{\rm ref}$ for the DG in each period could be expressed as follows: equation (13) as shown at the bottom of the page where T_1 represented the duration time for the part where $Q_{\rm ref}$ was not equal to zero, and f was the instantaneous frequency at the beginning of each period. It has to be noted that the value of f is equal to that of f_0 during islanding for the DG operating at unity power factor. Therefore, the method actually detected the load's resonance frequency to calculate the value of $Q_{\rm ref}$ after islanding. According to (13), $Q_{\rm ref}$ for the DG in different frequency conditions was shown in Fig. 7.

For the DG operating at unity power factor, the rated value of $Q_{\rm ref}$ is zero. Essentially, the aforementioned PRV methods periodically added the bilateral or unilateral reactive power disturbance on the DG's reactive power reference to force the frequency to deviate during islanding. When these methods were applied to single DG, they could detect islanding effectively. However, when they were applied to multiple DGs, the synchronization of the variations could not be guaranteed in both methods. Owing to the averaging effect, they might fail to detect islanding for the system with multiple DGs.

According to the method in [23], Fig. 8 illustrated the separate and total reactive power variations for the system with two DGs, where the reactive power variation on the DG2 lagged behind that on the DG1 and f_0 is 50 Hz. Therefore, when islanding occurred, the variation on the DG1 forced the frequency to increase earlier and the frequency was larger than 50 Hz when the variation on the DG2 started. Accordingly, the magnitude of the variation on the DG2 was less than $5\%P_{\rm DG2}$. Assuming that the active power references of both DGs were same ($P_{\rm DG1} = P_{\rm DG2}$), the maximum value of the total reactive power variation after islanding was smaller than $10\%P_{\rm DG1}$ and its duration time

$$Q_{\rm ref} = \begin{cases} \left.\begin{array}{ll} P_{\rm DG}Q_f\left(\dfrac{f}{50.5}-\dfrac{50.5}{f}\right), & 50\,{\rm Hz} \le f < 50.5\,{\rm Hz} \\ P_{\rm DG}Q_f\left(\dfrac{f}{49.5}-\dfrac{49.5}{f}\right), & 49.5\,{\rm Hz} < f < 50\,{\rm Hz} \end{array}\right\} & 0 \le t < T_1 \\ 0, & T_1 \le t < T_{\rm dis} \end{cases} \tag{13}$$

was less than T_1. Therefore, the reactive power variation was not sufficient to force the frequency to deviate outside its limits and the method failed to detect islanding. The analysis of the performance of the method in [22] for multiple-DG operation is similar.

In addition, both aforementioned methods were prepared for the DG operating at unity power factor. If the DG is generating reactive power as well to improve the load's power factor and voltage quality, the value of $Q_{\rm dis}$ will be unpredictable as analyzed in Section II-A. Moreover, the reactive power disturbances on multiple DGs might be still asynchronous. Therefore, these methods would be no longer applicable for the DG of this kind as well.

III. Proposed Islanding Detection Method Based on Reactive Power Disturbance

In order to improve the performance of islanding detection methods that are based on the reactive power disturbance, following three problems have to be solved: 1) the method has to be applicable for both the DG operating at unity power factor and that generating reactive power as well; 2) the disturbance on the DG is better to be reduced as much as possible during normal operation and it also has to be sufficient to drive the frequency outside its threshold limits after islanding; and 3) the synchronization of the disturbances on different DGs has to be guaranteed.

As analyzed in Section II, the relationships among f_0, f_i, and $Q_{\rm dis}$ are different for these two kinds of DGs. Considering different relationship characteristics, the method proposed in this paper can detect islanding effectively for both kinds of DGs. In order to solve the second problem mentioned earlier, two sets of reactive power disturbances, which have different amplitudes and duration time, are designed in the proposed method. The FSORPD is periodic with small amplitudes, whereas the magnitude of the SSORPD is sufficient to force the frequency to deviate outside its threshold limits during islanding. In addition, considering all the possible frequency variation characteristics with the FSORPD after islanding, three criterions are designed for switching the disturbance from the FSORPD to the SSORPD. Since DGs located at different positions can detect the same frequency variation characteristics, the SSORPDs on different DGs can be synchronously activated without the need of communication. In the following parts, the proposed method is introduced in detail.

A. FSORPD and Three Criterions for Switching the Disturbance From the FSORPD to the SSORPD

The reactive power disturbance itself can break the reactive power balance during islanding, thus making the elimination of the NDZ possible. In addition, the design of the FSORPD also has to comply with following two principles: 1) reducing disturbance as much as possible during normal operation and 2) forming criterions for starting the SSORPD after islanding. In order to meet aforementioned requirements, the FSORPD is designed to contain two parts whose amplitudes are $Q_{\rm dis1}$ and $2Q_{\rm dis1}$, respectively, and it is added on the DG's rated reactive power reference periodically. The value of $Q_{\rm dis1}$ is equal to either $Q_{\rm dis11}$ or $Q_{\rm dis12}$, which depends on the frequency at the beginning of the FSORPD. $Q_{\rm dis1}$ can be expressed as follows: equation (14) as shown at the bottom of the page where $\Delta f_{\rm set}$ is a preset positive value and f is the instantaneous frequency at the beginning of the FSORPD. Moreover, the duration time of the first part is the same as that of the second part.

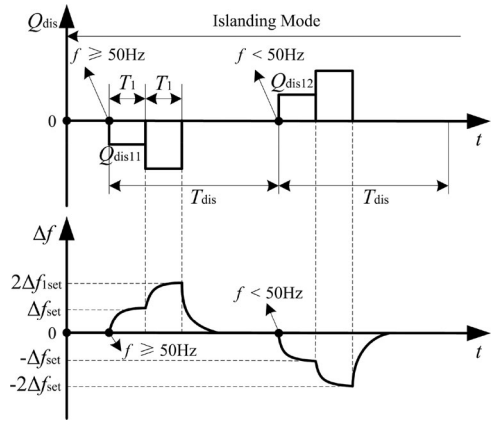

Fig. 9. FSORPD with different values of f and corresponding frequency variation during islanding.

Fig. 9 illustrates the FSORPD with different values of f and corresponding frequency variation during islanding, respectively. The FSORPD causes the sudden mismatch of the reactive power during islanding and accordingly there is a transient response of the frequency [22]. The duration time of the frequency transient process can be represented by $T_{\rm tra}$.

According to the analysis in Section II, if the frequency is equal to or larger than 50 Hz when the FSORPD starts, its value will be forced to be no less than $(50 + \Delta f_{\rm set})$ Hz with the disturbance $Q_{\rm dis11}$ or $(50 + 2\Delta f_{\rm set})$ Hz with the disturbance $2Q_{\rm dis11}$ during islanding. Similarly, if the frequency is smaller than 50 Hz when the FSORPD begins, its value will be forced to be less than $(50 - \Delta f_{\rm set})$ Hz with the disturbance $Q_{\rm dis12}$ or $(50 - 2\Delta f_{\rm set})$ Hz with the disturbance $2Q_{\rm dis12}$. The deduction above is appropriate for the DG operating at unity power factor and the DG generating active and reactive power simultaneously with f_0 being set at 50 Hz. The aim of the FSORPD is not to drive the frequency to deviate outside its threshold limits

$$Q_{\rm dis1} = \begin{cases} Q_{\rm dis11} = P_{\rm DG} Q_f \left(\dfrac{50}{50 + \Delta f_{\rm set}} - \dfrac{50 + \Delta f_{\rm set}}{50} \right), & f \geq 50\,{\rm Hz} \\ Q_{\rm dis12} = P_{\rm DG} Q_f \left(\dfrac{50}{50 - \Delta f_{\rm set}} - \dfrac{50 - \Delta f_{\rm set}}{50} \right), & f < 50\,{\rm Hz} \end{cases} \tag{14}$$

TABLE I
CRITERIONS FOR SWITCHING THE DISTURBANCE FROM THE FSORPD TO THE SSORPD

Criterion	Content	Corresponding Condition
First	1) $f >$ 50.3 Hz or $f <$ 49.7 Hz; 2) its duration time is no less than $T_{\rm dur}$.	The FSORPDs are synchronous or the nonsynchronization is not serious.
Second	1) The SOAFV is periodic; 2) its cycle time is equal to $T_{\rm dis}$.	1) The FSORPDs are asynchronous; 2) some FSORPDs overlap with each other.
Third	1) The SOAFV satisfies equation (16); 2) the frequency variation is not zero.	1) The FSORPDs are asynchronous; 2) a certain FSORPD does not overlap with the others.

during islanding. Therefore, in order to reduce the disturbance during normal operation, $\Delta f_{\rm set}$ is no need to be larger than 0.25 Hz and it can be set at 0.2 Hz. Accordingly, if the FSORPDs on multiple DGs are synchronous when islanding occurs, the frequency will be eventually no less than 50.4 Hz or smaller than 49.6 Hz at the end of the FSORPD. Therefore, the first criterion to start the SSORPD is that the frequency is larger than 50.3 Hz or smaller than 49.7 Hz with the duration time no less than $T_{\rm dur}$. The upper threshold of the frequency in this criterion is a little bit smaller than 50.4 Hz and the lower one is larger than 49.6 Hz. Therefore, the nonsynchronization of the FSORPDs that is not serious is still allowed for the system with multiple DGs. Moreover, the purpose of the configuration of $T_{\rm dur}$ is to avoid frequently starting the SSORPD during normal operation due to the frequency fluctuation caused by the switching of loads or other equipment, thus reducing the reactive power disturbance as well.

For the system with multiple DGs, the premise of the first criterion is the synchronization of the FSORPDs. However, this premise cannot be guaranteed and the total disturbance might not be adequate to force the frequency to be larger than 50.3 Hz or smaller than 49.7 Hz during islanding. Moreover, when the DG generates both active and reactive power simultaneously, f_0 cannot be obtained in advance as well and it might not be equal to 50 Hz. In a word, the first criterion might not be satisfied during islanding. Therefore, more criterions are needed. There are two possible conditions that the FSORPDs are asynchronous: 1) the overlap region exists among the FSORPDs on several DGs and 2) the FSORPD on a certain DG does not overlap with the FSORPDs on the other DGs. Considering the frequency variation characteristics that correspond to aforementioned two conditions during islanding, another two criterions are designed.

As for the condition that the FSORPDs on some DGs overlap with each other, the total disturbance, which is the sum of these FSORPDs, is periodic as well. Moreover, the period duration time is the same as that of the FSORPD, which is equal to $T_{\rm dis}$. Corresponding to this total disturbance, the frequency deviates periodically during islanding. Therefore, the second criterion is designed based on this characteristic. In order to obtain precise measurement of the frequency variation, the sum of absolute frequency variation (SOAFV) $\Delta F_{\rm tot}$ is utilized and its value can be calculated by

$$\begin{cases} \Delta F_{\rm tot} = \sum_{n=1}^{N} |\Delta f_n| \\ \Delta f_n = f_n - 50 \\ N = \dfrac{T_{\rm win}}{T_{\rm sam}} \end{cases} \tag{15}$$

where $T_{\rm win}$ is the measurement window size, $T_{\rm sam}$ is the sampling time, N is the total sampling number in a measurement window, and f_n is the nth sampling value of the instantaneous frequency. The second criterion is that the time difference between two adjacent maximum values of $\Delta F_{\rm tot}$ is equal to $T_{\rm dis}$.

On the other hand, when the FSORPD on a certain DG does not overlap with the FSORPDs on the other DGs, the frequency variation characteristic caused by this FSORPD is almost the same as that shown in Fig. 9. The only difference is that the absolute value of frequency variation is smaller than $\Delta f_{\rm set}$ or $2\Delta f_{\rm set}$ because of the inadequate reactive power mismatch. Actually, $\Delta F_{\rm tot}$ is the area of the frequency variation within a measurement window. It can be seen from Fig. 9 that following relationships are satisfied at the end of the second part of this FSORPD:

$$\begin{cases} \Delta F_{\rm tot.2} = \Delta F_{\rm tot.1} + N \cdot |\Delta f_2| / 2 \\ |\Delta f_1| > 0 \\ |\Delta f_2| > 0 \end{cases} \tag{16}$$

where $\Delta F_{\rm tot.2}$ and Δf_2 represent the SOAFV and the frequency variation at current time, $\Delta F_{\rm tot.1}$ and Δf_1 represent the SOAFV and the frequency variation T_1 before the current time, respectively. Moreover, the value of $T_{\rm win}$ has to be either equal to that of T_1 or no more than that of $(T_1 - T_{\rm tra})$. Therefore, (16) is configured as the third criterion for disturbance switching.

The aforementioned three criterions for switching the disturbance from the FSORPD to the SSORPD are shown in Table I. The second and third criterions complement each other, which can reduce the starting time of the SSORPD. Moreover, these two criterions reflect the frequency variation characteristics corresponding to the FSORPD during islanding. Therefore, when either of these two criterions is satisfied, the operation mode can be preliminarily judged as suspected islanding.

B. SSORPD and Two Criterions for Islanding Determination

Since DGs located at different positions have the same frequency variation characteristics, the SSORPDs on different DGs can be activated at the same time without the need of communication. The SSORPD is designed to be able to force the frequency to deviate outside its threshold limits and determine islanding eventually. Therefore, compared with the FSORPD, the SSORPD has larger amplitude. Moreover, its value for the DG operating at unity power factor is different from that for the DG generating both active and reactive power simultaneously.

TABLE II
CRITERIONS FOR ISLANDING DETERMINATION

Criterion	Content	Suitable Application
First	1) $f >$ 50.5 Hz or $f <$ 49.3 Hz; 2) its duration time is no less than T_{dur}.	1) The DG operating at unity power factor; 2) the DG generating both active and reactive power.
Second	1) The SOAFV satisfies equation (19); 2) the frequency variation is not zero.	The DG generating both active and reactive power.

As for the DG operating at unity power factor, the amplitude of the SSORPD can be expressed as follows:

$$Q_{\mathrm{dis2}} = \begin{cases} Q_{\mathrm{dis21}} = P_{\mathrm{DG}} Q_f \left(\dfrac{50}{50+0.6} - \dfrac{50+0.6}{50} \right), & f \geq 50\,\mathrm{Hz} \\ Q_{\mathrm{dis22}} = P_{\mathrm{DG}} Q_f \left(\dfrac{50}{50-0.8} - \dfrac{50-0.8}{50} \right), & f < 50\,\mathrm{Hz}. \end{cases} \tag{17}$$

In addition, the duration time of the SSORPD is also set at T_1. When islanding occurs, the frequency is eventually no less than 50.6 Hz or smaller than 49.2 Hz. In case of nonislanding switching evens, which may transiently impose a significant frequency deviation as well, the duration time of above abnormal frequency condition has to be no less than T_{dur} to determine islanding. It has to be noted that the SSORPD is not periodic. If the SSORPD is activated by false islanding, it will be replaced by the FSORPD again after its duration.

As for the DG generating both active and reactive power simultaneously, f_0 is unknown in advance and it cannot be calculated after islanding. Therefore, the SSORPD for the DG of this kind contains two parts, which have the same duration time T_1 but different amplitudes. The amplitude of the first part can be expressed as follows: equation (18) as shown at the bottom of the page.

This disturbance can force the frequency to deviate outside its thresholds for the load whose resonant frequency is equal to 50 Hz. The magnitude of the second part is set at $3Q_{\mathrm{dis2}}$, which can force the frequency to exceed its thresholds for the load whose resonant frequency is equal to 300 Hz as analyzed in Section II. Therefore, the SSORPD is sufficient to detect islanding when f_0 is within the range between 50 and 300 Hz. For the condition that f_0 is out of this range, additional criterion is needed to determine islanding. Owing to different disturbance amplitudes, the steady frequency variation corresponding to the second part is three times as much as that corresponding to the first part during islanding. Therefore, the additional criterion can be designed as follows:

$$\begin{cases} \Delta F_{\mathrm{tot.22}} = 3\Delta F_{\mathrm{tot.11}} \\ |\Delta f_{11}| > 0 \\ |\Delta f_{22}| > 0 \end{cases} \tag{19}$$

where $\Delta F_{\mathrm{tot.22}}$ and Δf_{22} represent the SOAFV and the frequency variation at the end of the second part of the SSORPD, $\Delta F_{\mathrm{tot.11}}$ and Δf_{11} represent the SOAFV and the frequency variation at the end of the first part of the SSORPD, respectively. It is important to note that the value of T_{win} for $\Delta F_{\mathrm{tot.22}}$ and $\Delta F_{\mathrm{tot.11}}$ should be no more than that of $(T_1 - T_{\mathrm{tra}})$.

In conclusion, two criterions for islanding determination are shown in Table II. For the DG operating at unity power factor, the first criterion is enough. However, both criterions have to be configured to complement each other for the DG generating both active and reactive power simultaneously. If either criterion is satisfied, islanding can be confirmed.

TABLE III
TIME VARIABLES AND THEIR MEANINGS

Time Variable	Meaning
T_1	The duration time of each part in both the FSORPD and the SSORPD.
T_{dis}	The period time of the FSORPD.
T_{win}	The measurement window size for SOAFV calculation.
T_{tra}	The transient time of frequency deviation from a steady value to another steady one.
T_{dur}	The duration time of the abnormal frequency state.

C. Time Variable Design

The time variables utilized in the proposed method are listed in Table III and this part introduces the design of their values.

The frequency can be obtained from the PLL, which is based on the input of three single-phase voltages at the PCC. The authors in [22] analyzed the transient characteristics of the PLL in detail when the operation mode transferred from grid-connected operation to islanding. With the same PLL structure as shown in [22], T_{tra} is approximately 87.1 ms. In order to avoid the

$$Q_{\mathrm{dis2}} = \begin{cases} Q_{\mathrm{dis21}} = P_{\mathrm{DG}} Q_f (50-50.6) \left(\dfrac{50}{50 \cdot 50.6} + \dfrac{1}{50} \right), & f \geq 50\,\mathrm{Hz} \\ Q_{\mathrm{dis22}} = P_{\mathrm{DG}} Q_f (50-49.2) \left(\dfrac{50}{50 \cdot 49.2} + \dfrac{1}{50} \right), & f < 50\,\mathrm{Hz}. \end{cases} \tag{18}$$

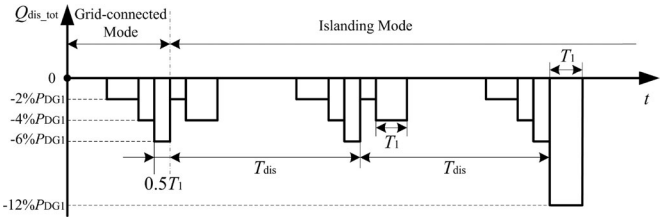

Fig. 10. Schematic diagram of the maximum islanding detection time.

influence of the frequency transient process, T_1 should be larger than 87.1 ms and it can be set at 100 ms, which was also recommended in [22] and [23]. Therefore, the duration time of the frequency in the steady state is approximately 12.9 ms and $T_{\rm win}$ can be set at 10 ms.

The most serious condition for islanding detection is that there are no active and reactive power mismatches between the generation of the DG and the load's consumption. When the reactive power disturbance is not added, the frequency is still its rated value 50 Hz after islanding. Accordingly, the maximum detection time of the proposed method appears in this condition as well. According to the first and third criterions, the needed time to start the SSORPD after islanding is no more than $T_{\rm dis}$. That is because both criterions are designed based on the frequency variation characteristics corresponding to the synchronous FSORPDs on different DGs or the FSORPD on a certain DG. However, based on the second criterion, the needed time for disturbance switching is at least equal to $T_{\rm dis}$. Assuming that the active power references of two DGs are same ($P_{\rm DG1} = P_{\rm DG2}$) and the FSORPD on the DG2 lags $1.5T_1$ behind that on the DG1, Fig. 10 illustrates the maximum detection time of the proposed method when islanding occurs. The FSORPD on the DG2 overlaps with that on the DG1. The maximum value of the total reactive power disturbance is $6\%P_{\rm DG1}$. However, its duration time $0.5T_1$ is less than $T_{\rm tra}$ and the frequency fails to exceed 50.3 Hz. Therefore, both the first and third criterions for starting the SSORPD cannot be satisfied in this condition. As shown in Fig. 10, when islanding occurs, the total reactive power disturbance ($Q_{\rm dis_{tot}}$) just misses its maximum value. Thus, it needs $2T_{\rm dis}$ to meet the second criterion. Then, the SSORPDs are added on both DGs synchronously and the frequency deviates to 50.6 Hz eventually. Therefore, the maximum detection time is a little bit smaller than $(2T_{\rm dis} + T_{\rm tra} + T_{\rm dur})$. According to IEEE Std.929 and IEEE Std.1547, islanding is required to be detected in 2 s and the limitation of $T_{\rm dis}$ can be expressed as follows:

$$2T_{\rm dis} + T_{\rm tra} + T_{\rm dur} \le 2. \tag{20}$$

With $T_{\rm tra}$ and $T_{\rm dur}$ being equal to 87.1 and 10 ms, respectively, $T_{\rm dis}$ is no more than 951.5 ms.

D. Implementation Steps of the Proposed Method

The proposed islanding detection method is easy to implement. The flowchart of the proposed method is presented in Fig. 11. First, two sets of reactive power disturbances, three

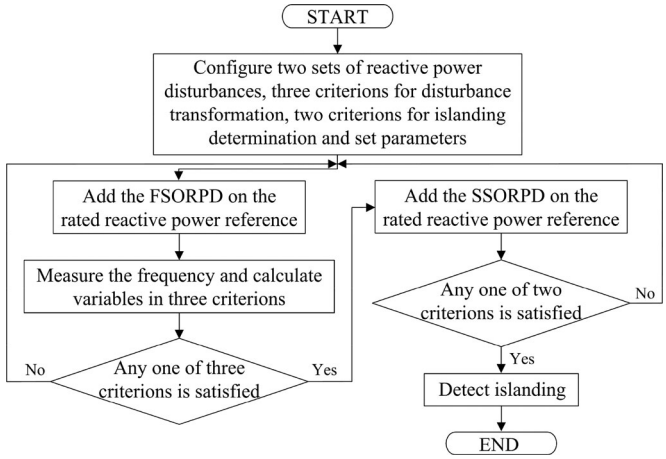

Fig. 11. Flowchart of the proposed islanding detection method.

criterions for disturbance switching and two criterions for islanding determination have to be configured. Relative parameters are set in advance as well. Generally, the FSORPD is added on the rated reactive power reference of the DG. If any of three criterions for disturbance switching is satisfied, the SSORPD will take the place of the FSORPD. Then, if either of two criterions for islanding detection is met, islanding will be determined. Otherwise, the SSORPD will be replaced by the FSORPD after its duration time.

Constant *RLC* load is generally considered as the hardest detectable condition for an islanding detection method and it is recommended in the generic system to examine the islanding detection methods' performance. In [31], different types of loads were modeled by varying the load's voltage and frequency dependence parameters and the performance of the OVP/UVP and OFP/UFP methods with different load models was analyzed. It was found that the load's voltage and frequency-dependence parameters have no effect on the amount of frequency deviation. Moreover, for the constant power load, since the DG was under constant power control when islanding occurred and there was no voltage dependence, the voltage collapsed. Therefore, the islanding can be easily detected for the load of this kind according to the passive OVP/UVP methods [32]. As for the motor load, the experiment results in [23] showed that only the passive OFP/UFP method could realize islanding detection even though there were no active and reactive power mismatches.

In addition, according to (14), (17), and (18), the value of $Q_{\rm dis}$ depends on the DG's active power output $P_{\rm DG}$. If the value of $P_{\rm DG}$ is equal to zero after islanding, the value of $Q_{\rm dis}$ will be zero as well. Therefore, the proposed method cannot detect islanding for this condition. However, according to (1), the PCC voltage is also zero in this case. Since the voltage collapses, the passive OVP/UVP method can easily detect islanding in this situation.

Therefore, the proposed method and the passive OVP/UVP and OFP/UFP methods can form the redundancy configuration and this configuration can realize islanding detection effectively and reliably for the system with different kinds of loads.

TABLE IV
PARAMETERS OF THE STUDY SYSTEM

	Parameters	Values
Grid	Voltage	400 V
	Frequency	50 Hz
	Grid Resistance	0.1 Ω
	Grid Inductance	1.5915 mH
DG Inverter Controller	K_{p1}/K_{i1}	0.025/2
	K_{p2}/K_{i2}	1.5/0.01
	$P_{\rm ref}$	200 kW

TABLE V
LOAD PARAMETER SETTING FOR DIFFERENT TEST CASES IN PART A

Case	R/Ω	L/mH	C/μF	f_0/Hz
1	0.8	1.0186	9947.2	50
2	0.8	1.0145	9907.6	50.2
3	0.8	1.0105	9868.2	50.4
4	0.8	1.0227	9987.1	49.8
5	0.8	1.0268	10027.4	49.6

IV. PERFORMANCE OF THE PROPOSED ISLANDING DETECTION METHOD

In this section, several test cases are simulated on the power systems computer-aided design (PSCAD)/Electro magnetic transient in DC system (EMTDC) based on the system in Fig. 1. The main parameters of the grid and the DG are given in Table IV, where K_{p1}/K_{i1} and K_{p2}/K_{i2} represent the PI parameters for the outer power control loop and the inner current loop, respectively. Moreover, two kinds of DGs are considered and the only difference between them is that their rated reactive power references are different. Both kinds of DGs' active power references are set at 200 kW.

On the other hand, the performance of the proposed islanding detection method is tested under a wide variety of *RLC* load conditions. T_1 and $T_{\rm dis}$ in the FSORPD are set at 100 and 600 ms, respectively, and $T_{\rm dur}$ in the criterions is set at 10 ms. The islanding is initiated at $t = 0.3$ s and the frequency is the rated value 50 Hz before islanding. According to the proposed method, if islanding occurs, it will be detected with the SSORPD in the theory. Therefore, after the duration time of the SSORPD is over, the FSORPD is no longer added on the DG again in the simulation.

A. Performance of the Proposed Method for the DG Operating at Unity Power Factor

If the DG operates at unity power factor, its rated reactive power reference will be 0 Var. According to changing the values of the load's inductance and capacitance, different values of f_0 can be created. As shown in Table V, five sets of values of parameters *R*, *L*, and *C* are configured with Q_f equal to 2.5. As for the DG operating at unity power factor, the active power mismatch during islanding has no impact on the frequency variation. Thus, in these five test cases, the values of parameter *R* are set at 0.8 Ω to match the DG's output active power. Moreover, without considering islanding, a new cycle of the FSORPD is designed to be added on the reactive power reference at $t = 0.5$ s in each case. Therefore, if the system operates normally, there will be no reactive power disturbance before 0.5 s.

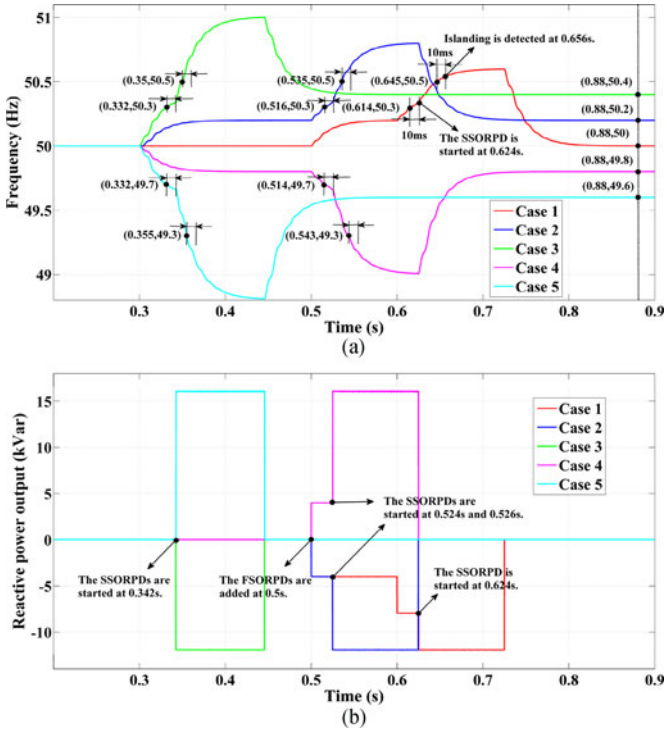

Fig. 12. Simulation results for loads with different values of f_0 during islanding (a) The PCC frequency (b) The DG's reactive power output.

Fig. 12 illustrates the PCC frequency and the DG's reactive power output during islanding in each test case of Part A. It can be noted from Fig. 12(a) that frequencies deviate outside the threshold limits in all five cases and islanding can be detected with different detection time.

In case 1, the frequency begins to exceed 50.3 Hz at 0.614 s due to the second part of the FSORPD. In the following 10 ms, it stays above 50.3 Hz. Therefore, the first criterion for disturbance switching is satisfied at 0.624 s and the SSORPD replaces the FSORPD accordingly. Afterwards, the frequency is larger than its upper threshold 50.5 Hz from 0.646 s and islanding is eventually determined at 0.656 s. Compared with case 1, frequencies in the following four cases start to deviate once islanding occurs. That is because the values of f_0 are not equal to 50 Hz, which can be seen from frequencies at 0.88 s (there are no reactive power disturbances at 0.88 s). In cases 2 and 4, the values of f_0 are still within the thresholds in the first criterion for disturbance switching. However, the first part of the FSORPD is sufficient to force the frequency to meet the first criterion compared with case 1. Accordingly, the disturbance switching from the FSORPD to the SSORPD is realized earlier and the detection time in these two cases is smaller than that in case 1. In cases 3 and 5, the values of f_0 are both beyond the thresholds in the first criterion for disturbance switching. Thus, the SSORPDs in these two cases are activated fastest and islanding is detected in the least time.

TABLE VI
SIMULATION RESULTS FOR DIFFERENT TEST CASES IN PART A

Case	f_0/Hz	Startup time of the SSORPD/ms	Detection result	Detection time/ms
1	50	324	detected	356
2	50.2	226	detected	245
3	50.4	42	detected	60
4	49.8	224	detected	260
5	49.6	42	detected	70

According to Fig. 12(a), the startup time of the SSORPDs, detection results and detection time for these five cases are shown in Table VI. It can be seen from Table VI that the proposed method can detect islanding for the loads with different values of f_0. For the condition that no reactive power mismatch exists after islanding ($f_0 = 50$ Hz), the detection time is longest, whereas it is still much less than the specified 2 s given in IEEE Std.1547. In addition, if the frequency is closer to its threshold limits before the FSORPD starts, the detection time will be shorter.

On the other hand, the performance of the proposed method for unbalanced loads is also examined. As presented in [14] and [25], the load imbalance is simulated by varying the load phase resistance. Based on case 1 in Table V, following three conditions are considered: 1) in case A, only the resistance of phase a is set at 97% of its rated value; 2) in case B, only the resistance of phase c is set at 103% of its rated value; 3) in case C, resistances of phase *a* and phase *c* are set at 97% and 103% of the rated value, respectively. With the DG adopting the general constant power control strategy, the PCC frequency and the DG's reactive power output during islanding in each aforementioned test case are shown in Fig. 13.

It can be inferred from Fig. 13(a) that frequencies in all three cases eventually deviate outside the upper threshold 50.5 Hz and the duration time of this condition is longer than 10 ms. Therefore, the proposed method is capable of detecting islanding effectively in load imbalance conditions as well. Moreover, it also can be seen from Fig. 13(a) that the fluctuation range of the PCC frequency is larger for the more unbalanced load. In order to detect islanding rapidly and reliably, the magnitude of the SSORPD can be set a little bit larger for the serious unbalanced load.

B. Performance of the Proposed Method for the DG Generating Active and Reactive Power Simultaneously

As analyzed in [25], for the DG generating active and reactive power simultaneously, even though there was no reactive power mismatch between the DG and its local load during normal operation, active power mismatch could cause reactive power mismatch during islanding, thus driving the frequency to deviate and making the islanding detection easier. The active power mismatch can be created by changing the value of the load's resistance. Without considering the disturbance, the rated reactive power reference for the DG is set at 100 kVar in this part. The reactive power mismatch is realized via varying the values of the load's inductance and capacitance. As shown in Table VII, five sets of values of parameters *R*, *L*, and *C* are configured as well

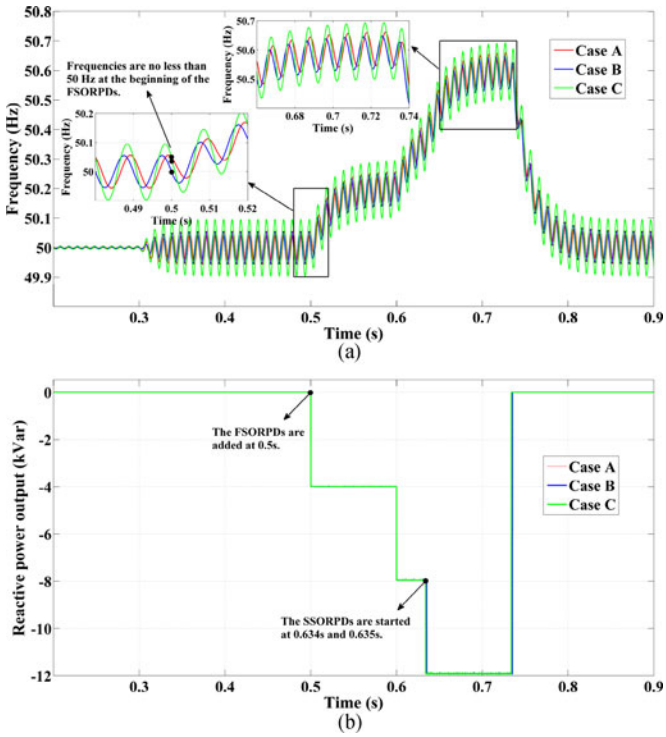

Fig. 13. Simulation results for unbalanced loads (a) The PCC frequency (b) The DG's reactive power output.

TABLE VII
LOAD PARAMETER SETTING FOR DIFFERENT TEST CASES IN PART B

Case	R/Ω	L/mH	C/μF	f_0/Hz	ΔP_{nor}/kW	ΔQ_{nor}/kVar
1	0.8	0.9218	9002.1	55.3	0	0
2	0.7619	0.9218	9002.1	55.3	10	0
3	0.8421	0.9218	9002.1	55.3	−10	0
4	0.8	0.9145	8930.7	55.7	0	8
5	0.8	0.9292	9074.1	54.8	0	−8

in this part. ΔP_{nor} and ΔQ_{nor} in Table VII represent the active power mismatch and the reactive power mismatch between the DG and the load during normal operation, respectively. The values of Q_f in cases 1, 4, and 5 are equal to 2.5. Cases 2 and 3 are designed based on case 1 and the only difference among them is that they have different values of ΔP_{nor}.

Fig. 14 illustrates the PCC frequency and the DG's reactive power output during islanding in each case of Part B. When islanding occurs, the value of the active power mismatch remains the same. However, the reactive power mismatches become different in cases 2 and 3 after islanding. That is because the active power mismatches are not equal to zero and the PCC voltages have changed in both cases. Accordingly, compared with the frequency in case 1, it can be seen from Fig. 14(a) that the frequency starts to descend in case 2 or rise in case 3 once islanding occurs. Therefore, the SSORPDs in cases 2 and 3 are activated earlier than that in case 1, which means islanding can be detected in less time in cases 2 and 3. The islanding detection time for these three cases is 357, 241, and 239 ms, respectively. Though the active power generated from the DG matches that

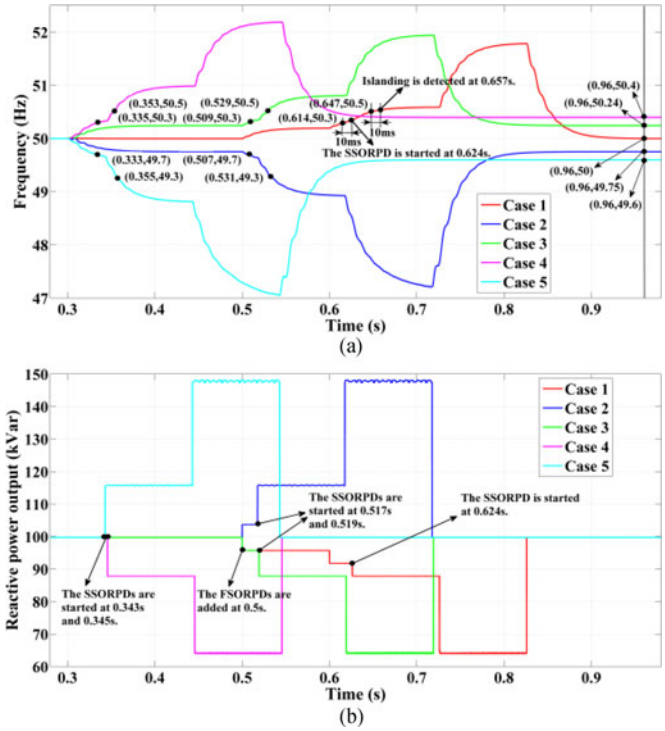

Fig. 14. Simulation results during islanding for the DG generating active and reactive power simultaneously (a) The PCC frequency (b) The DG's reactive power output.

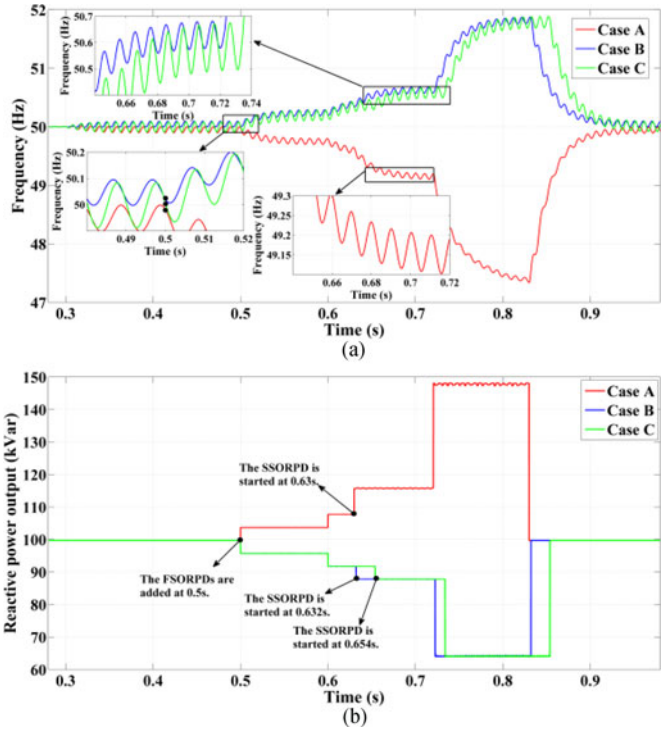

Fig. 15. Simulation results for unbalanced loads (a) The PCC frequency (b) The DG's reactive power output.

consumed by the load in cases 4 and 5, there are reactive power mismatches to force the frequency to deviate after islanding. As shown in Fig. 14(a), frequencies in these five cases have been in the steady state at $t = 0.96$ s. At this moment, frequencies in cases 4 and 5 are beyond the threshold limits in the first criterion for starting the SSORPD while those in cases 1, 2, and 3 are not. Therefore, the SSORPDs in cases 4 and 5 are started shortly after islanding while those in the other three cases are not activated until the FSORPDs are added on the rated reactive power references. Accordingly, the islanding detection time in cases 4 and 5 is 63 and 65 ms, respectively, which is shorter than that in the other three cases. In addition, the values of f_0 in these five cases are a little bit larger than 50 Hz. That means the needed reactive power disturbances to force the frequencies to exceed the threshold limits are approximately the same as that for the load whose resonant frequency is equal to 50 Hz. Therefore, islanding can be detected during the first part of the SSORPD in all these five cases.

The performance of the proposed method with the unbalanced load is examined as well in this part. Based on case 1 in Table VII, the same three conditions as introduced in Part A are simulated by changing the load's resistance. Fig. 15 shows the simulation results in these three cases. It can be seen from Fig. 15(a) that frequencies in all three conditions deviate outside the threshold limits and the duration time of this condition is longer than 10 ms. Therefore, for the DG generating active and reactive power simultaneously, the proposed method can also effectively detect islanding when the three single-phase loads are unbalanced.

C. *Comparison of the Performance of the Proposed Method With that of the Methods in [22] and [23] for the DG Operating at Unity Power Factor Under Multiple-DG Operation Mode*

The performance of the proposed islanding detection method is further tested on the system with multiple DGs. Moreover, it is also compared with the performance of the methods proposed in [22] and [23], which have been described in Section II. For multiple-DG operation in this part, both DGs connect together with a centralized load at the PCC. Either DG operates at unity power factor with its rated active power equal to 200 kW. The parameters *R*, *L*, and *C* are adjusted to consume both DGs' rated output power with Q_f equal to 2.5. Therefore, their values are 0.4 Ω, 0.5093 mH, and 19894.4 μF, respectively. In addition, $T_{+Q}/T_{-Q}/T_1$ and $T_{\rm dis}$ are set at 100 and 600 ms, respectively, as well in the methods proposed in [22] and [23].

The synchronization of the FSORPDs in this paper and the disturbances in [22] and [23] on different DGs cannot be guaranteed. Considering the possible conditions of these disturbances on both DGs, following three scenarios are designed: 1) in scenario A, the disturbances are added on the rated reactive power references of both DGs simultaneously at $t = 0.5$ s; 2) in scenario B, the disturbances are not added at the same time, but they overlap with each other. Two cases are simulated in this scenario and the disturbance on the DG2 lags behind that on the DG1 for 80 and 180 ms, respectively, in these two cases; and 3) in scenario C, the disturbance on the DG2 lags behind that on the DG1 for 250 ms, and therefore, the disturbances do not overlap with each other. It has to be noted that the duration time of the disturbance proposed in [23] is 100 ms, while that in this

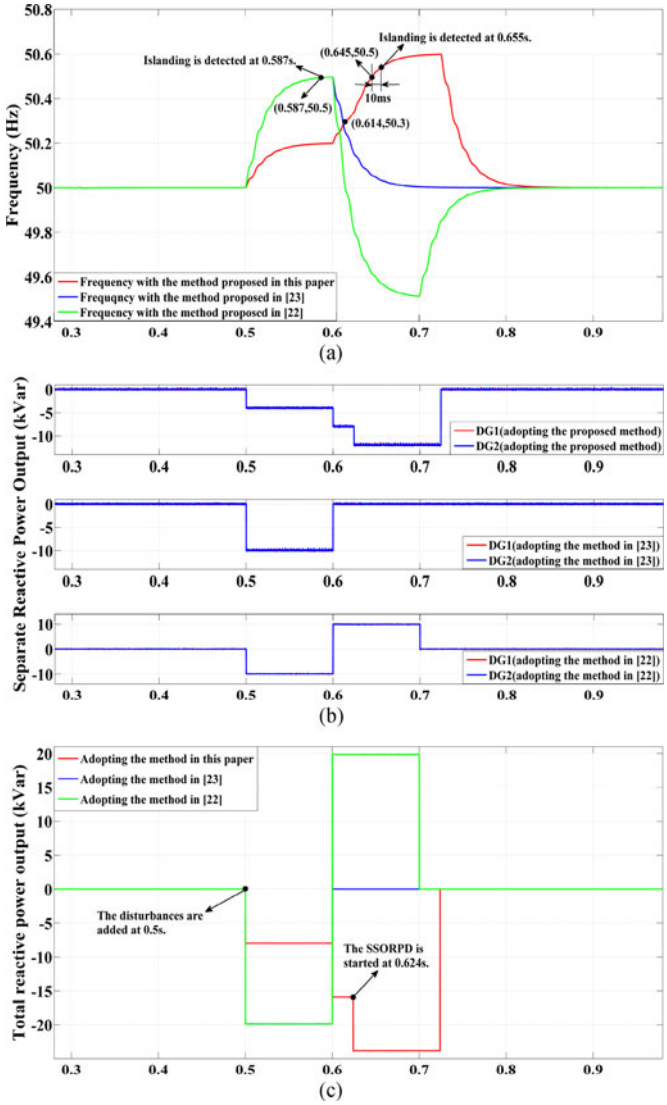

Fig. 16. Simulation results with three methods in scenario A (a) The PCC frequency (b) Separate reactive power output (c) The DG's total reactive power output.

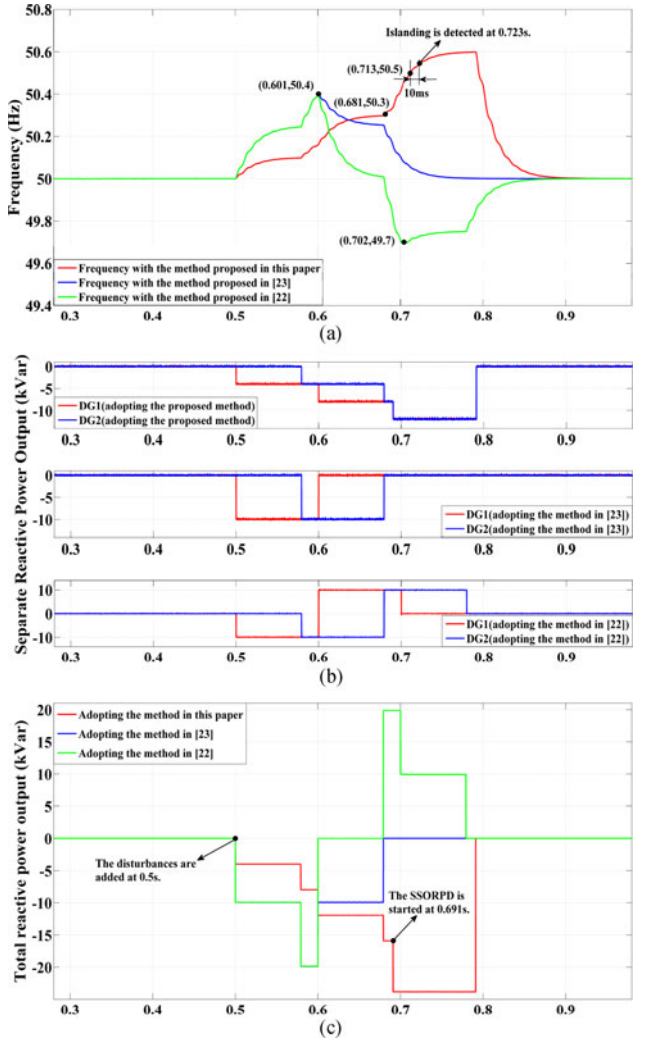

Fig. 17. Simulation results in scenario B (the lag time is 80 ms) (a) The PCC frequency (b) Separate reactive power output (c) The DG's total reactive power output.

paper and in [22] is 200 ms. Therefore, when the disturbance on the DG2 lags behind that on the DG1 for 180 ms in scenario B, the disturbances do not overlap with each other with the method proposed in [23]. For comparison, this situation is simulated as well in scenario B.

Fig. 16 shows the PCC frequency and the DGs' total reactive power output in scenario A according to different methods. It can be seen from Fig. 16(a) that islanding can be detected with all these three methods in this scenario. Though the detection time with the method proposed in this paper is a little bit longer than that with the other two methods, the possibility of false detection can be eliminated using additional duration time criterion and the disturbance amplitudes are also smaller during normal operation.

Fig. 17 illustrates the simulation results in scenario B with the lag time equal to 80 ms. Since the disturbances on both DGs are asynchronous in this scenario, the reactive power mismatches are insufficient to force frequencies to deviate outside the threshold limits with the methods proposed in [22] and [23] and these two methods fail to detect islanding. However, it can be seen from Fig. 17 that the overlap part of the FSORPDs can still drive the frequency to be larger than 50.3 Hz with the method proposed in this paper, thus the SSORPDs are added on both DGs synchronously. Accordingly, the frequency exceeds its upper threshold 50.5 Hz and islanding is detected eventually. Compared with that in scenario A, the detection time in this case is a little bit longer. That's because the first criterion for disturbance switching needs longer time to be satisfied, which is caused by the nonsynchronization of the FSORPDs on both DGs.

Fig. 18 illustrates the PCC frequency and the DGs' total reactive power output in scenario B with the lag time equal to 180 ms. It can be seen from Fig. 18(a) that frequencies with the methods proposed in [22] and [23] are still within the normal range in this case and both methods fail to detect islanding again.

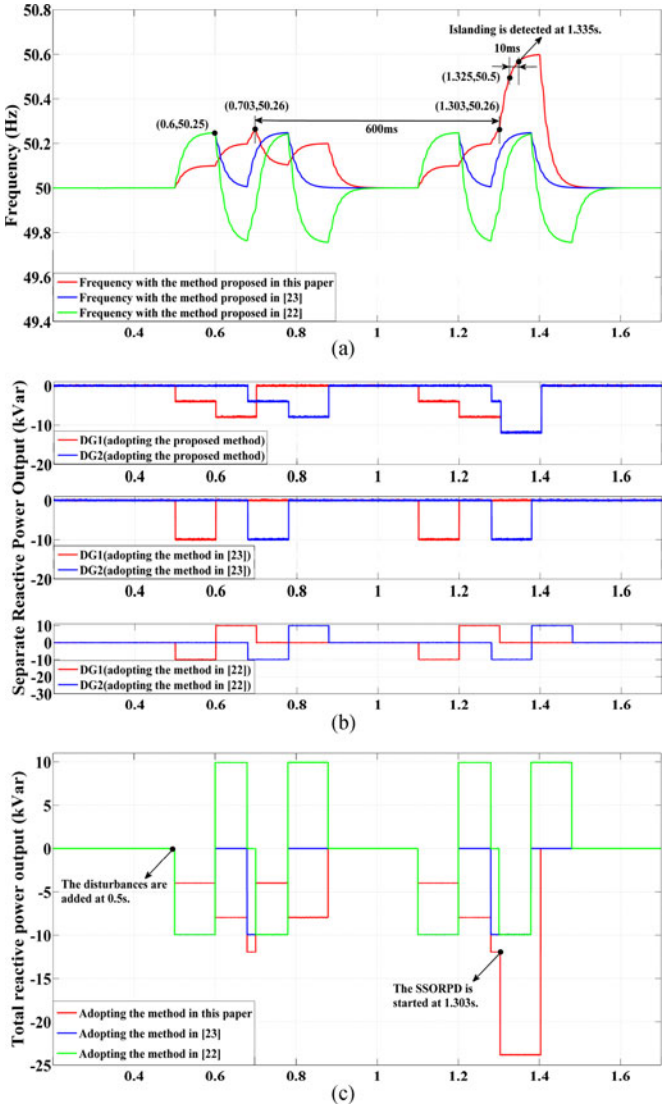

Fig. 18. Simulation results in scenario B (the lag time is 180 ms) (a) The PCC frequency (b) Separate reactive power output (c) The DG's total reactive power output.

With the longer lag time in this case, the duration time for the overlap part of the FSORPDs is only 20 ms with the method proposed in this paper. As shown in Fig. 18(a), the maximum value of the frequency caused by this overlap part is 50.26 Hz, which is less than 50.3 Hz. It means that the first criterion for disturbance switching is not satisfied. However, the frequency varies periodically in this case. In the second criterion for disturbance switching, the measurement window $T_{\rm win}$ is set to be equal to 10 ms. The PSCAD/EMTDC simulation model is a discrete model with the sampling time equal to 50 μs. Accordingly, the total number of samples N in a measurement window is 200. Fig. 19 illustrates the SOAFV after deliberately blocking the SSORPDs. As shown in Fig. 19, the time difference between two adjacent maximum values of $\Delta F_{\rm tot}$ is 600 ms, which is equal to $T_{\rm dis}$. Therefore, the second criterion for disturbance switching is satisfied at $t = 1.303$ s and the SSORPDs on both DGs are activated simultaneously. Eventually, islanding can still be detected within 1.035 s with the method proposed in this paper, even though the FSORPDs on both DGs are asynchronous in this case.

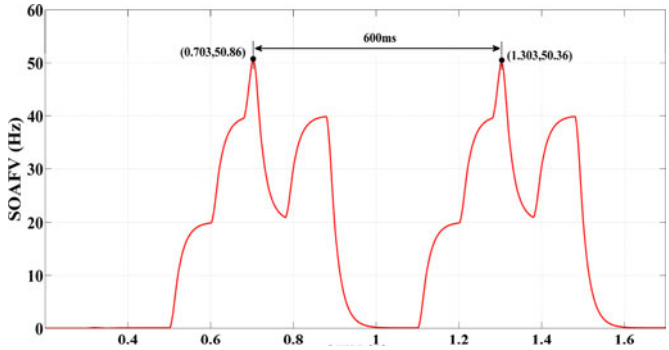

Fig. 19. SOAFV after deliberately blocking the SSORPDs in scenario B (the lag time is 180 ms).

Fig. 20 shows the simulation results with three methods in scenario C. It can be seen that frequencies with the methods proposed in [22] and [23] are within the normal range after islanding, whereas the frequency with the method proposed in this paper eventually exceeds its upper threshold. Therefore, when the disturbances on both DGs are asynchronous and they do not overlap with each other, the method proposed in this paper can still effectively detect islanding (the detection time is 440 ms in scenario C), while those in [22] and [23] cannot.

Fig. 21 illustrates the SOAFV after deliberately blocking the SSORPDs in scenario C. It can be seen from Figs. 20(a) and 21 that the frequency and the SOAFV at $t = 0.7$ s are 50.2 and 39.85 Hz, respectively, and the SOAFV at $t = 0.6$ s is 19.88 Hz. Therefore, the third criterion for disturbance switching, which is expressed as (16), is approximately satisfied at $t = 0.7$ s. Accordingly, The SSORPDs on both DGs are activated simultaneously, which creates sufficient reactive power mismatch to force the frequency to deviate outside its upper limit.

For the DG generating active and reactive power simultaneously under multiple-DG operation mode, the proposed method can still performs well and detect islanding effectively. The frequency variation characteristics for the DG of this kind in these three scenarios are nearly the same as those for the DG operating at unity power factor. Therefore, the simulation results are not presented here.

D. Performance of the Voltage Disturbance in Grid-Connected Mode

In grid-connected condition, the PCC voltage can be calculated approximately by the following equation [26], [30]:

$$V_{\rm PCC} = V_{\rm Grid} - \frac{P_{\rm Grid} R_g}{V_{\rm PCC}} - \frac{Q_{\rm Grid} X_g}{V_{\rm PCC}} \qquad (21)$$

where $V_{\rm Grid}$ and $R_g + jX_g$ are the voltage of the grid and the equivalent line impedance at the grid side, respectively. Assuming that the DG completely compensates the load's power consumption, the value of $Q_{\rm Grid}$ is equal to zero without the reactive power disturbance. However, when the rectangular disturbance is added on the DG, $Q_{\rm dis}$ and $Q_{\rm Grid}$ have opposite

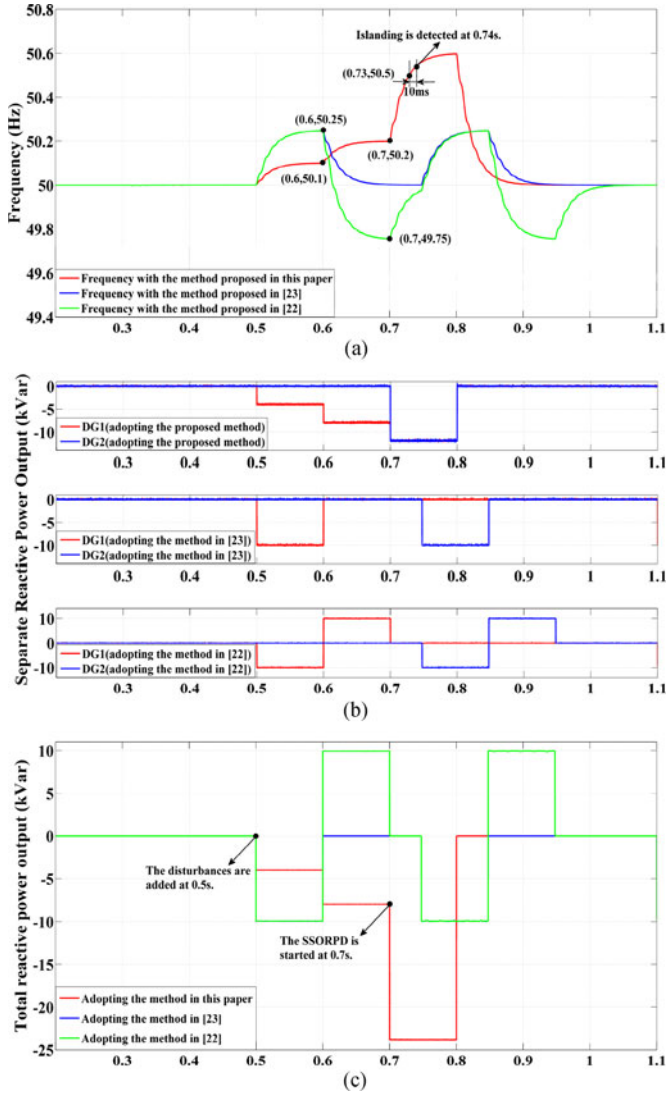

Fig. 20. Simulation results with three methods in scenario C (a) The PCC frequency (b) Separate reactive power output (c) The DG's total reactive power output.

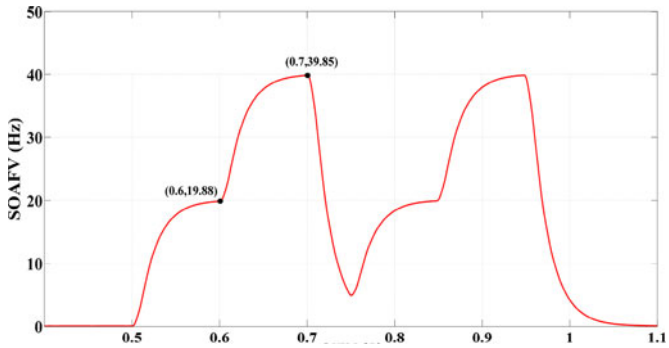

Fig. 21. SOAFV after deliberately blocking the SSORPDs in scenario C.

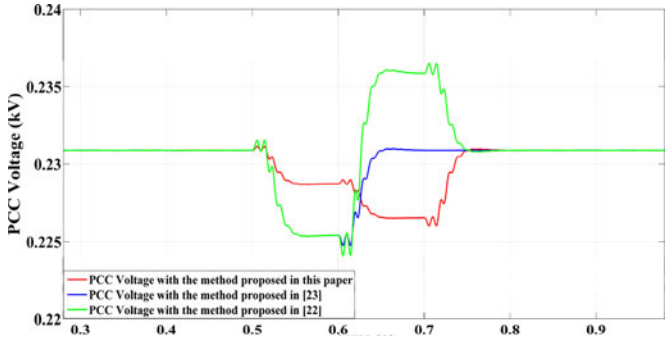

Fig. 22. Voltage disturbance results in grid-connected mode.

signs and the same absolute value. Accordingly, the PCC voltage fluctuates during this process. Therefore, the reactive power variation causes the voltage disturbance and the maximum voltage deviation depends on the value of $Q_{\rm dis}$.

The performance of the voltage disturbance is tested in this part. The absolute values of $Q_{\rm dis}$ are both at least $5\%P_{\rm DG}$ according to the methods in [22] and [23], whereas it is smaller with the proposed method. As analyzed in Section III-A, the absolute value of $Q_{\rm dis}$ depends on $\Delta f_{\rm set}$, whose value is less than 0.25 Hz. If $\Delta f_{\rm set}$ is set at 0.2 Hz, the absolute value of $Q_{\rm dis}$ will be $4\%P_{\rm DG}$. Fig. 22 illustrates the voltage disturbance results of these three methods. It can be seen from Fig. 22 that the maximum voltage deviation with the proposed method is smaller than those adopting the methods in [22] and [23].

V. Conclusion

Under constant power control, the inverter-based DG can either operate at unity power factor or generate both active and reactive power simultaneously. For the DG generating both active and reactive power simultaneously, this paper analyzes the relationship between the reactive power disturbance and the frequency variation during islanding. According to the basic relationship analysis, this paper presents an innovative islanding detection method for the DG of both kinds based on perturbing the DG's reactive power output and this method is very easy to implement.

In the proposed method, two sets of reactive power disturbances are designed. They have different magnitudes and duration time for different purposes. Basically, the FSORPD is added on the DG. It is periodic and it aims to destroy the reactive power balance between the DG and the load after islanding, and then, activate the SSORPD. Therefore, the magnitudes of the FSORPD are small so as to reduce the impact on the system during normal operation. However, the SSORPD has large magnitude. Its purpose is to force the frequency to deviate outside its threshold limits to determine islanding no matter there are power mismatches or not between the DG's rated power output and the load's consumption. Thus, the method can eliminate the NDZ.

When the FSORPDs are added on different DGs, they might be asynchronous. Considering all the possible frequency variation characteristics with these FSORPDs after islanding, three

criterions are designed as well for switching the disturbance from the FSORPD to the SSORPD on the DG. Moreover, DGs located at different positions can detect the same frequency variation characteristics no matter what the operation mode is, which guarantees the synchronization of the SSORPDs on different DGs without the need of communication. Accordingly, the proposed method can effectively and reliably detect islanding for multiple-DG operation. Simulation results verify that the proposed method performs well on islanding detection.

REFERENCES

[1] H. B. Puttgen, P. R. MacGregor, and F. C. Lambert, "Distributed generation: Semantic hype or the dawn of a new era?," *IEEE Power Energy Mag.*, vol. 1, no. 1, pp. 22–29, Jan./Feb. 2003.

[2] P. P. Barker and R. W. de Mello, "Determining the impact of distributed generation on power systems: Part 1—Radial distribution systems," in *Proc. IEEE Power Eng. Soc. Summer Meeting*, Jul. 2000, pp. 1645–1656.

[3] *IEEE Recommended Practice for Utility Interface of Photovoltaic (PV) Systems*, IEEE Standard 929-2000, Apr. 2000.

[4] *IEEE Standard for Interconnecting Distributed Resources with Electric Power Systems*, IEEE Standard 1547-2003, Jul. 2003.

[5] R. A. Walling and N. W. Miller, "Distributed generation islanding—Implications on power system dynamic performance," in *Proc. IEEE Power Eng. Soc. Summer Meeting*, Jul. 2002, pp. 92–96.

[6] G. Hernandez-Gonzalez and R. Iravani, "Current injection for active islanding detection of electronically-interfaced distributed resources," *IEEE Trans. Power Del.*, vol. 21, no.3, pp. 1698–1705, Jul. 2006.

[7] A. Timbus, A. Oudalov, and N. M. Ho Carl, "Islanding detection in smart grids," in *Proc. IEEE Energy Convers. Congr. Expo.*, Sep. 2010, pp. 3631–3637.

[8] D. Reigosa, F. Briz, C. Blanco, P. Garcia, and J. M. Guerrero, "Active islanding detection for multiple parallel-connected inverter-based distributed generators using high-frequency signal injection," *IEEE Trans. Power Electron.*, vol. 29, no. 3, pp. 1192–1199, Mar. 2014.

[9] F. De Mango, M. Liserre, A. D. Aquila, and A. Pigazo, "Overview of anti-islanding algorithms for PV systems. Part I: Passive methods," in *Proc. IEEE Power Electron. Motion Control Conf.*, Aug. 2006, pp. 1878–1883.

[10] Z. Ye, A. Kolwalkar, Y. Zhang, P. Du, and R. Walling, "Evaluation of anti-Islanding schemes based on nondetection zone concept," *IEEE Trans. Power Electron.*, vol. 19, no. 5, pp. 1171–1176, Sep. 2004.

[11] H. H. Zeineldin, E. F. EI-Saandany, and M. M. A. Salama, "Impact of DG interface control on islanding detection and nondetectionzones," *IEEE Trans. Power Del.*, vol. 21, no. 3, pp. 1515–1523, Jul. 2006.

[12] F. De Mango, M. Liserre, and A. D. Aquila, "Overview of anti-islanding algorithms for PV systems. Part II: Active methods," in *Proc. IEEE Power Electron. Motion Control Conf.*, Aug. 2006, pp. 1884–1889.

[13] J. H. Kim, J. G. Kim, Y. H. Ji, Y. C. Jung, and C. Y. Won, "An islanding detection method for a grid-connected system based on the Goertzel algorithm," *IEEE Trans. Power Electron.*, vol. 26, no. 4, pp. 1049–1055, Apr. 2011.

[14] H. Karimi, A. Yazdani, and R. Iravani, "Negative-sequence current injection for fast islanding detection of a distributed resource unit," *IEEE Trans. Power Electron.*, vol. 23, no. 1, pp. 298–307, Jan. 2008.

[15] A. Yafaoui, B. Wu, and S. Kouro, "Improved active frequency drift anti-islanding detection method for grid connected photovoltaic systems," *IEEE Trans. Power Electron.*, vol. 27, no. 5, pp. 2367–2375, May 2012.

[16] L. A. C. Lopes and H. L. Sun, "Performance assessment of active frequency drifting islanding detection methods," *IEEE Trans. Energy Convers.*, vol. 21, no. 1, pp. 171–180, Mar. 2006.

[17] H. Vahedi and M. Karrari, "Adaptive fuzzy Sandia frequency-shift method for islanding protection of inverter-based distributed generation," *IEEE Trans. Power Del.*, vol. 28, no. 1, pp. 84–92, Jan. 2013.

[18] E. J. Estebanez, V. M. Moreno, A. Pigazo, M. Liserre, and A. DellAquila, "Performance evaluation of active islanding - detection algorithms in distributed-generation photovoltaic systems: Two inverters case," *IEEE Trans. Ind. Electron.*, vol. 58, no. 4, pp. 1185–1193, Apr. 2011.

[19] L. A. C. Lopes and Y. Z. Zhang, "Islanding detection assessment of multi-inverter systems with active frequency drifting methods," *IEEE Trans. Power Del.*, vol. 23, no. 1, pp. 480–486, Jan. 2008.

[20] H. H. Zeineldin, E. F. EI-Saandany, and M. M. A. Salama, "Islanding detection of inverter-based distributed generation," *Proc. IEE*, vol. 153, no. 6, pp. 644–652, Nov. 2006.

[21] H. H. Zeineldin, "A *Q–f* droop curve for facilitating islanding detection of inverter-based distributed generation," *IEEE Trans. Power Electron.*, vol. 24, no. 3, pp. 665–673, Mar. 2009.

[22] J. Zhang, D. H. Xu, G. Q. Shen, Y. Zhu, N. He, and J. Ma, "An improved islanding detection method for a grid-connected inverter with intermittent bilateral reactive power variation," *IEEE Trans. Power Electron.*, vol. 28, no. 1, pp. 268–278, Jan. 2013.

[23] Y. Zhu, D. H. Xu, N. He, J. Ma, J. Zhang, Y. F. Zhang, G. Q. Shen, and C. S. Hu, "A novel RPV (reactive-power-variation) antiislanding method based on adaptive reactive power perturbation," *IEEE Trans. Power Electron.*, vol. 28, no. 11, pp. 4998–5012, Nov. 2013.

[24] P. Gupta, R. S. Bhatia, and D. K. Jain, "Average absolute frequency deviation value based active islanding detection technique," *IEEE Trans. Smart Grid*, vol. 6, no. 1, pp. 26–35, Jan. 2015.

[25] X. L. Chen and Y. L. Li, "An islanding detection algorithm for inverter-based distributed generation based on reactive power control," *IEEE Trans. Power Electron.*, vol. 29, no. 9, pp. 4672–4683, Sep. 2014.

[26] Y. Zhou, H. Li, and L. Liu, "Integrated Autonomous voltage regulation and islanding detection for high penetration PV applications," *IEEE Trans. Power Electron.*, vol. 28, no. 6, pp. 2826–2841, Jun. 2013.

[27] F. J. Lin, Y. S. Huanh, K. H. Tan, J. H. Chiu, and Y. R. Chang, "Active islanding detection method using *d*-axis disturbance signal injection with intelligent control," *IET Generation, Transmiss. Distrib.*, vol. 7, pp. 537–550, May 2013.

[28] P. G. Barbosa, L. G. B. Rolim, E. H. Watanabe, and R. Hanitsch, "Control strategy for grid-connected DC-AC converters with load power factor correction," *Proc. IEE*, vol. 145, no. 5, pp. 487–491, Sep. 1998.

[29] S. Huang and F. Pai, "Design and operation of grid-connected photovoltaic system with power-factor control and active islanding detection," *Proc. IEE*, vol. 148, no. 3, pp. 243–250, May 2001.

[30] E. Demirok, D. Sera, R. Teodorescu, P. Rodriguez, and U. Borup, "Evaluation of the voltage support strategies for the low voltage grid connected PV generators," in *Proc. IEEE Energy Convers. Congr. Expo.*, Sep. 2010, pp. 710–717.

[31] H. H. Zeineldin and J. L. Kirtley, "Performance of the OVP/UVP and OFP/UFP method with voltage and frequency dependent loads," *IEEE Trans. Power Del.*, vol. 24, no. 2, pp. 772–778, Apr. 2009.

[32] H. H. Zeineldin and J. L. Kirtley, "Islanding operation of inverter based distributed generation with static load models," in *Proc. IEEE Power Energy Soc. General Meeting*, Jul. 2008, pp. 1–6.

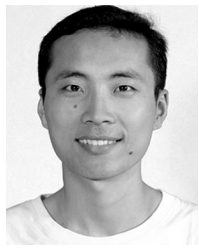

Xiaolong Chen was born in Henan, China, in 1985. He received the B.S., M.S., and Ph.D. degrees in electrical engineering from Tianjin University, Tianjin, China, in 2010, 2012, and 2015, respectively.

He is currently a Lecturer in the Department of Electrical Engineering and Automation, Tianjin University, Tianjin, China. His research interests include protection and control of the microgrid and distribution network containing the distributed generation.

Yongli Li was born in Hebei, China, in 1963. She received the B.S. and M.S. degrees in electrical engineering from Tianjin University, Tianjin, China, in 1984 and 1987, respectively, and the Ph.D. degree in electrical engineering from UniversiteLibre de Bruxelles, Brussel, Belgium, in 1993.

She is currently a Professor in the Department of Electrical Engineering and Automation, Tianjin University, and also a member of CIGRE SC-B5. Her research interests include fault analysis of power system and fault diagnosis of electrical equipment, protection and adaptive reclosing of EHV/UHV transmission system, and protection and control of the microgrid and distribution network.